

2048. A new rockfill dynamic characteristics analogy method using statistic relationship

Yufeng Jia¹, Shichun Chi², Biao Xiang³

^{1,2}Institute of Earthquake Engineering, Dalian University of Technology, Dalian, China

^{1,2}State Key Laboratory of Coastal and Offshore Engineering, Dalian University of Technology, Dalian, Liaoning, 116024, China

³POWERCHINA Kunming Engineering Corporation, Kunming, China

²Corresponding author

E-mail: ¹jiayf130@dlut.edu.cn, ²schchi@dlut.edu.cn, ³103931114@qq.com

Received 23 December 2015; received in revised form 22 April 2016; accepted 20 May 2016

DOI <http://dx.doi.org/10.21595/jve.2016.1676>

Abstract. Dynamic numerical analysis by the finite element method (FEM) is widely used for the seismic performance analysis of earth-rockfill dams. The dynamic characteristics of soil, which can be measured by dynamic tests, determine the results of the FEM analysis. However, due to their high costs and long duration, dynamic tests are not feasible for many small- to middle-scale earth-rockfill dams. As a result, the analogy method is employed. Because the traditional analogy method is highly dependent on personal experience, it lacks objective and accurate orientations. In this paper, a new method to analogize the dynamic characteristics of rockfill by prototype monitoring and statistic curves is developed. To examine its effectiveness, the dynamic parameters of a middle-scale concrete-face rockfill dam (CFRD) were analogized. The results of the dynamic FEM analysis agree well with the general rules which were shown in the earthquake response and the dynamic FEM analysis response of the same type of CFRD

Keywords: rockfill, dynamic characteristics analogy method, prototype monitoring.

1. Introduction

On May 12, 2008, an earthquake of magnitude 8.0 occurred in Wenchuan, which is located in Sichuan Province, China. After the earthquake, 2,666 dams in eight provinces suffered different extents of damage [1]. On July 11, 2008, the Chinese government announced that certain dams, which satisfy one of the conditions listed in Table 1, that have been built or that are under construction undergo special seismic design censorship, which is primarily dependent on dynamic analysis with the finite element method (FEM). Before the Wenchuan earthquake, only a few large dams satisfying the conditions mandated by the Chinese Specifications for Seismic Design of Hydraulic Structures should take dynamical analysis with the FEM. As new conditions listed in Table 1 are more comprehensive, numerous middle-scale dams should use dynamic analysis with the FEM to analyze the seismic safety of the dam. In July 2010, the government launched reinforcement work for unsafe small-scale reservoirs; approximately 5,400 unsafe small-scale dams required reinforcement design according to the results of seismic dynamic analysis by the FEM.

Table 1. Dynamic analysis of the dams with the FEM: conditions

Conditions of the specifications	Maximum reservoir capacity $\geq 10^9 \text{ m}^3$	Design intensity ≥ 7.0
	Install capacity $\geq 1,200 \text{ MW}$	
	Maximum height $\geq 70 \text{ m}$	
	Liquefiable soil located in foundation	
Conditions of the new order	Maximum reservoir capacity $\geq 10^8 \text{ m}^3$	Design intensity ≥ 7 degree or design earthquake acceleration $\geq 0.1 \text{ g}$
	Install capacity $\geq 300 \text{ MW}$	
	Maximum height $\geq 70 \text{ m}$	Liquefiable soil located in foundation

The dynamic characteristics of the soil in earth-rockfill dams (generally acquired by dynamic tests, such as dynamic triaxial tests, dynamic simple shear tests, cyclic torsional shear tests,

resonant column tests, and shear wave velocity tests) determine the results of the FEM analysis. Due to high costs, long periods, and limited service, dynamic tests have only been conducted for some of the dams. The dynamic characteristics of soil for the majority of small- to middle-scale dams are determined by the analogy method which refers to using or making adjustment to the similar soil dynamic characteristics as the analogized soil dynamic characteristics, according to the soil parameters such as material, dry density, grading curve, and so on. It is highly dependent on personal experience and lacks objective and accurate orientations. A simple, reliable, and effective method to analogize soil dynamic characteristics should be developed for small- to middle-scale dams using dynamic FEM analysis.

The dynamic characteristics of soil in earth-rockfill dams can be generally described by an equivalent linear viscoelastic model, which incorporates the initial dynamic elastic shear modulus G_{max} , normalized modulus reduction relationships $G/G_{max} \sim \gamma$ (G is dynamic shear modulus and γ is dynamic shear strain), and the damping ratio ξ versus γ relationships $\xi \sim \gamma$. G_{max} can be obtained at small-strain cyclic loading (γ is typically less than 0.001 %), when the soil is in an elastic state. Numerous scholars have performed experiments to examine G_{max} , which is a key factor in soil dynamic characteristics [2,3]. $G/G_{max} \sim \gamma$ and $\xi \sim \gamma$ are also important factors. Seed et al. developed ranges of $G/G_{max} \sim \gamma$ and $\xi \sim \gamma$ for sandy and gravelly soils [3]. Rollins et al. provided best-fit curves and standard deviation bounds of $G/G_{max} \sim \gamma$ and $\xi \sim \gamma$ for gravel [4]. Kong et al. proposed ranges of $G/G_{max} \sim \gamma$ and $\xi \sim \gamma$ for rockfill [5]. The author developed $G/G_{max} \sim \gamma$ and $\xi \sim \gamma$ statistic curves for rockfill, which were applied in the dynamic analysis of two middle-scale CFRDs. The details were published in the 15th World Conference on Earthquake Engineering (15WCEE).

In this paper, a statistical relationship between G_{max} and Duncan and Chang's $E-B$ model parameters E_0 of rockfill was developed. According to prototype monitoring of a dam, E_0 of the rockfill were determined by a back analysis, which reflected the influence of construction. The G_{max} of rockfill can be analogized according to the statistical relationship and E_0 . According to the analogized G_{max} , $G/G_{max} \sim \gamma$ and $\xi \sim \gamma$ statistic curves of the rockfill, the $G/G_{max} \sim \gamma$ and $\xi \sim \gamma$ curves were analogized.

2. The analogy method of G_{max}

The G_{max} of soil is affected by many factors, such as particle size, material, gradation, confining pressure, fabric of soil skeleton, stress path, loading frequency, density, saturation, and temperature [2]. Different soils are affected by different factors. Thus, the G_{max} of clays, slits, sands, gravel soils, and rockfills should be described differently.

Seed et al. developed the empirical function of granular soils (sand and gravels) as:

$$G_{max} = 1000K_2 P_a \left(\frac{\sigma'_0}{P_a} \right)^{\frac{1}{2}}, \quad (1)$$

where K_2 is a shear modulus coefficient, which can be determined by the standard penetration test, σ'_0 is the mean effective confining pressure, P_a is the atmosphere [3].

Hardin and Kalinski modified the G_{max} empirical function of sand to estimate the G_{max} of gravelly soils as:

$$G_{ij}^e = \frac{OCR^k}{0.3 + 0.7e^2} \cdot \frac{S_{ij}}{2(1 + \nu^e)} P_a^{1-n} \cdot (\sigma'_{ii} \sigma'_{jj})^{\frac{n}{2}}, \quad (2)$$

where G_{ij}^e is the elastic shear modulus in three-dimensional formats, e is the void ratio, OCR is the over consolidation ratio, S_{ij} is the dimensionless elastic stiffness coefficient, σ'_{ii} is the principle stress, ν^e is the elastic Poisson's ratio, $f(D)$ is the particle size function, and k and n are model

parameters [6].

These empirical functions provided a practical method for determining the G_{max} of sand and gravel that corresponds to filter material and transition material in earth-rockfill dams. However, compared with the soils mentioned above, less effort has been applied to the G_{max} empirical function of rockfill. Rockfill, which is typically the largest component of an earth-rockfill dam, primarily affects the displacement of such dams. Furthermore, the G_{max} of rockfill measured in the laboratory using the maximum particle sizes in the samples are less than 60 mm. However, the maximum particle sizes of the rockfill in earth-rockfill dams may be as large as 1 m. The particle size affects the rockfill deformation properties. The rockfill shear deformation modulus increases as the particle sizes become larger for a given sample diameter and increases with the sample diameter for a given particle gradation [7]. Moreover, rockfill is produced by quarry blasting, the particles contain a few cracks, which result in considerable particle breakage. Particle breakage, which can be depicted by gradation curves, contributes to modified soil skeleton structures and affects the deformation characteristics of rockfill. Thus, the deformation characteristics of rockfill are influenced by compaction on a construction situ. The results of numerical simulation with the FEM in laboratory tests sometimes differ significantly from the results of prototype monitoring.

As noted previously, the G_{max} empirical function for rockfill does not incorporate the influences of particle size and construction on the site. Back analysis, which yields a more accurate numerical simulation, can be applied to determine the deformation characteristics of soil in dams. However, a complete seismic wave and corresponding seismic response of earth-rockfill were rarely collected, with the exception of a few earth-rockfill dams, such as the Li-yu-tan Dam, which was damaged but not completely destroyed by the Chi-Chi earthquake [8]. Dynamic back analysis of earth-rockfill is more difficult, and the dynamic characteristics of soils in dams are difficult to determine directly by dynamic back analysis. Conversely, the static back analysis method is widely applied. Complete deformation prototype monitoring of earth-rockfill dams is the predominant method for monitoring dam security. Static soil deformation characteristics determined by back analysis with prototype monitoring reflect the influences of construction and particle size, and provide more reliable evidence for G_{max} analogy.

The Duncan and Chang's $E-B$ model is a simple and practical nonlinear elastic static model. It is recommended by Chinese Design specification for rolled earth-rockfill dams (DL-5395-2007) to calculate displacement and stress of earth-rockfill dam. The Chinese Specification of soil test (SL237-1999) also provides techniques, which are used to determine soil parameters used in the Duncan and Chang's $E-B$ model according to triaxial test results. The Chinese engineering practices indicate that the Duncan and Chang's $E-B$ model can well simulate the settlements of earth-rockfill dams, whose computational accuracy satisfies the demand for engineering.

The Duncan and Chang's $E-B$ model suggested that the tangent modulus E_t is expressed as follows:

$$E_t = E_0(1 - R_f S)^2, \quad E_0 = K_e P_a \left(\frac{\sigma_3}{P_a}\right)^{n_e}, \quad S = \frac{(1 - \sin\varphi)(\sigma_1 - \sigma_3)}{2C\cos\varphi + 2\sigma_3\sin\varphi}, \quad (3)$$

where R_f is the failure ratio, S is the stress level, K_e is the modulus number, σ_3 is the minor principal stress, n_e is the modulus exponent, σ_1 is the major principal stress, φ is the friction angle, and c is the cohesion.

The nonlinear volume change is simulated using the bulk modulus, which is expressed as follows:

$$B = K_b P_a \left(\frac{\sigma_3}{P_a}\right)^m, \quad (4)$$

where K_b is the bulk modulus number and m is the bulk modulus exponent.

Table 2. Static and dynamic parameters of rockfill used in earth-rockfill dams

No.	Material	Dam height (m)	Rockfill mineralogy	Test type	Sample dia./ht. (cm)	Drainage condition
1	Manla rockfill [10]	76.3	Sandstone	TX/CTX	30/61	CD/SU
2	Zhangfeng rockfill DSS [11]	72.2	Sandstone	TX/CTX	30/75	CD/SU
3	Zhangfeng rockfill DSP [11]	72.2	Limestone	TX/CTX	30/75	CD/SU
4	Jilintai cushion [12]	157	Limestone	TX/CTX	30/60	CD/SU
5	Jilintai transition [12]	157	Limestone	TX/CTX	30/60	CD/SU
6	Yunpeng rockfill [13]	100	Limestone	NA	NA	NA
7	Yunpeng transition [13]	100	Sandstone	NA	NA	NA
8	Shiziping transition [13]	136	Limestone	NA	NA	NA
9	Tianshengqiao rockfill [14]	178	Granite	TX/NA	30/60	CD/NA
10	Main rockfill [15]	NA	Granite	TX/CTX	30/70	CD/SU
11	Secondary rockfill [15]	NA	Granite	TX/CTX	30/70	CD/SU
12	Shuangjiangkou transition [16]	314	NA	TX/CTX	30/70	CD/SU
13	Xieka secondary rockfill [17]	108	Granite	NA	NA	NA
14	Pubugou rockfill [18]	188	Sandstone	TX/CTX	30/60	CD/SU
15	Shiziping rockfill [13]	136	Granite	NA	NA	NA
16	Changheba rockfill [19]	240	Allgovite	TX/CTX	30/70	CD/SU
17	Xiliushui rockfill [20]	146.5	NA	NA	NA	NA
18	Xieka main rockfill [17]	108	Granite	NA	NA	NA
19	Shuangjiangkou upstream rockfill [16]	314	Limestone	TX/CTX	30/70	CD/SU
20	Zipingpu transition [21]	156	Limestone	TX/CTX	30/60	CD/SU
21	Zipingpu main rockfill [21]	156	Allgovite	TX/CTX	30/60	CD/SU
22	Xiliushui cushion [20]	146.5	Limestone	NA	NA	NA
23	Jiudianxia secondary rockfill [22]	136.5	Limestone	TX/NA	30/70	CD/NA
24	Transition 1 [15]	NA	Limestone	TX/CTX	30/70	CD/SU
25	Zipingpu cushion [21]	156	Granite	TX/CTX	30/60	CD/SU
26	Nuozhadu transition [23]	261.5	Granite	TX/CTX	30/70	CD/SU
27	Changheba transition [19]	240	Limestone	TX/CTX	30/70	CD/SU
28	Jiudianxia main rockfill [22]	136.5	Sand shale	TX/NA	30/70	CD/NA
29	Nuozhadu secondary rockfill [23]	261.5	Granite	TX/CTX	30/70	CD/SU
30	Nuozhadu main rockfill [23]	261.5	Limestone	TX/CTX	30/70	CD/SU
31	Jiudianxia transition [22]	136.5	Sand shale	TX/NA	30/70	CD/NA
32	Nuozhadu tertiary rockfill [23]	261.5	Limestone	TX/CTX	30/70	CD/SU
33	Jiudianxia cushion [22]	136.5	Limestone	TX/NA	30/70	CD/NA

The Mohr-Coulomb envelopes for cohesionless soils are curved to some extent, and a wider range of pressure corresponds to a greater curvature, particularly for gravel and rockfill. For example, at the bottom near the center of a large dam, the rockfill may be confined under such a large pressure that the friction angle is:

$$\varphi = \varphi_0 - \Delta\varphi \log\left(\frac{\sigma_3}{P_a}\right), \quad (5)$$

where φ_0 is the value of φ for $\sigma_3 = P_a$, and $\Delta\varphi$ is the reduction in φ for a 10-fold increase in σ_3 [9]. Thus, φ and c in Eq. (3) should be replaced by φ_0 and $\Delta\varphi$, respectively, for rockfill materials.

In the equivalent linear viscoelastic model, G_{max} can be expressed as:

$$G_{max} = K_g P_a \left(\frac{\sigma'_0}{P_a}\right)^{n_g}, \quad (6)$$

where K_g is the dimensionless elastic stiffness coefficient and n_g is the elastic stiffness exponent.

Although the E_0 in Eqs. (4) and (6) are similar because they both indicate the influence of stress on the deformation behavior of the soil, some differences remain. First, G_{max} is the secant modulus of the dynamic shear stress versus shear strain curves, whereas E_0 is the tangent modulus of the static shear stress versus axial strain curves. Second, G_{max} and E_0 are both determined by a modified straight-line function; the dynamic shear strain in the x-axial of G_{max} begins at 10^{-6} , whereas the static axial strain in the x-axial of E_0 begins at 10^{-3} . Third, G_{max} is determined in the undrained condition; thus, the volumetric strain cannot be tested; Poisson's ratio was generally estimated at 0.5 [4, 5]. Conversely, E_0 is determined in the drained condition. Finally, σ'_0 in the G_{max} function incorporates the influence of the consolidation ratio and is equivalent to σ_3 in the E_0 function when the consolidation ratio is equivalent to one. However, G_{max} and E_0 both represent elastic shear modulus and contain the same units. They are both expressed by the stress function, which indicates the pressure hardening characteristics of the soil. Furthermore, E_0 is the most important parameter in the E - B model that simulates deformation of the soil, which directly reflects the influence of construction on the displacement of an earth-rockfill dam.

Table 3. Static and dynamic parameters of rockfill used in earth-rockfill dams

No.	Dry density (g/cm ³)	Maximum grain size (mm)	Loading frequency (Hz)	Number of cycles	K_e	n_e	K_g	n_g
1	2.19	60	0.1	12	312	0.44	1,289	0.53
2	2.10	60	0.33	NA	316	0.46	1,628	0.47
3	2.09	60	0.33	NA	398	0.44	1,850	0.51
4	2.18	60	0.1	7	418	0.48	1,349	0.60
5	2.02	60	0.1	7	513	0.31	1,421	0.59
6	2.05	NA	NA	NA	585	0.58	2,216	0.61
7	2.20	NA	NA	NA	815	0.34	2,456	0.60
8	2.15	NA	NA	NA	860	0.48	1,000	0.60
9	2.15	60	NA	NA	900	0.35	2,379	0.48
10	2.26	60	0.33	NA	912	0.21	2,349	0.31
11	2.25	60	0.33	NA	944	0.20	2,379	0.30
12	2.09	60	0.1	3	960	0.25	2,019	0.31
13	2.09	NA	NA	NA	980	0.32	2,609	0.56
14	2.30	60	0.1	12-15	1,000	0.52	1,946	0.61
15	2.15	NA	NA	NA	1,000	0.50	1,200	0.69
16	2.13	60	0.33	3	1,000	0.24	2,714	0.47
17	2.15	NA	NA	NA	1,020	0.34	3,917	0.47
18	2.05	NA	NA	NA	1,040	0.30	2,902	0.57
19	2.12	60	0.1	3	1,050	0.25	4,142	0.42
20	2.25	60	NA	NA	1,085	0.38	3,184	0.51
21	2.16	60	NA	NA	1,089	0.33	3,784	0.42
22	2.23	NA	NA	NA	1,090	0.49	2,687	0.57
23	2.16	60	NA	NA	1,120	0.53	2,348	0.61
24	2.23	60	0.33	NA	1,161	0.24	2,530	0.34
25	2.30	60	NA	NA	1,274	0.44	3,051	0.51
26	2.04	60	0.33	3	1,300	0.27	1,651	0.47
27	2.02	40	0.33	3	1,318	0.24	1,604	0.39
28	2.20	60	NA	NA	1,400	0.53	2,902	0.57
29	2.15	60	0.33	3	1,530	0.18	2,324	0.34
30	2.00	60	0.33	3	1,425	0.26	2,570	0.35
31	2.25	60	NA	NA	1,500	0.55	3,338	0.63
32	2.09	60	0.33	3	1,551	0.18	2,324	0.34
33	2.28	40	NA	NA	1,750	0.43	3,533	0.57

So it would be an effective method to develop an empirical relationship between E_0 and G_{max} according to static and dynamic test results of the rockfill, which is similar to methods used

to resolve $G/G_{max} \sim \gamma$ and $\xi \sim \gamma$. According to the empirical relationship between E_0 and G_{max} , the G_{max} can be analogized using E_0 , which avoids the dynamic test. The author compiled the G_{max} and E_0 parameters of 33 types of rockfill that are used in 14 earth-rockfill dams, as listed in Table 3. According to the compiled reference, these parameters are all obtained by the laboratory test, whose details are listed in Table 2.

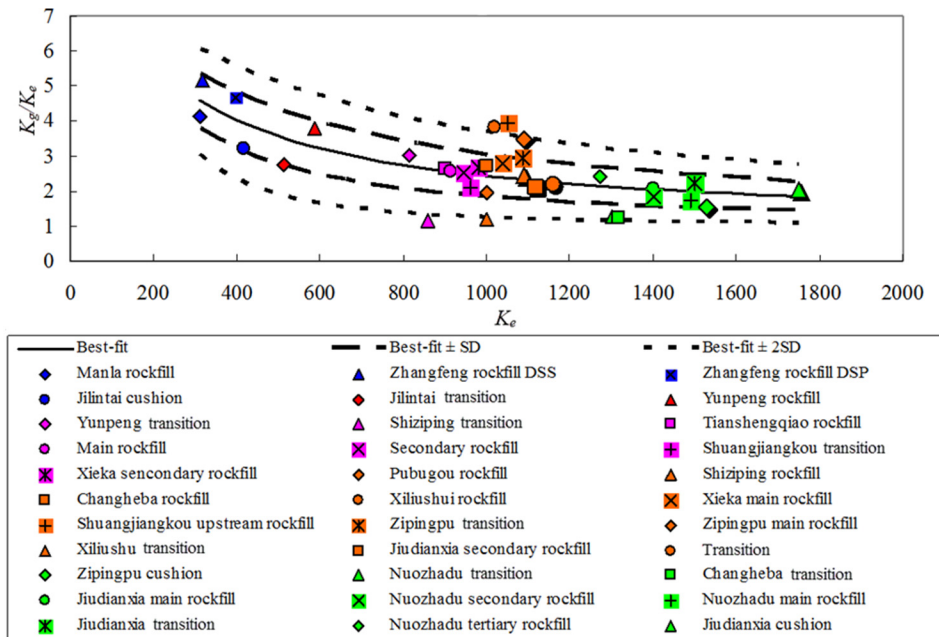


Fig. 1. Best-fit curve, the Best-fit curve \pm one and two SD, and data points that define K_g/K_e versus K_e relationships for 33 types of rockfills

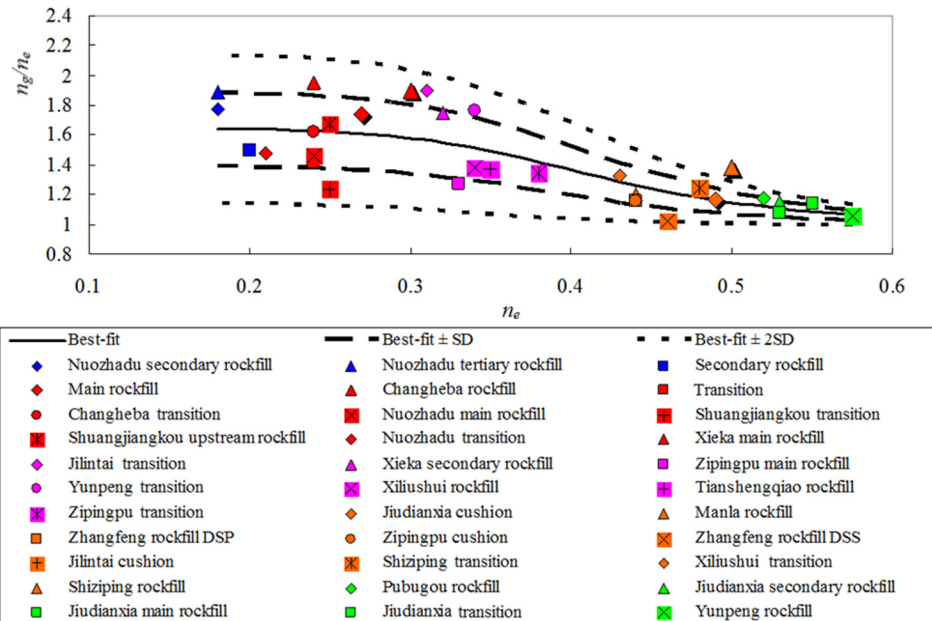


Fig. 2. Best-fit curve, the Best-fit curve \pm one and two SD, and data points that define n_g/n_e versus n_e relationships for 33 types of rockfills

The K_g/K_e versus K_e data points for the rockfills listed in Table 3 are plotted in Fig. 1, and n_g/n_e versus n_e data points are plotted in Fig. 2. The K_e and K_g represent the influences of material stiffness and soil skeleton structure on E_0 and G_{max} , respectively, whereas n_e and n_g reflect the sensitivity of soil skeleton structure to stress. As mentioned previously, K_g and n_g are typically acquired in an anisotropic consolidation state, whereas K_e and n_e are acquired in an isotropic consolidation state. This difference is eliminated by σ'_0 , which is equivalent to σ_3 when the consolidate ratio is equivalent to one. Thus, K_g and K_e are equivalent, and n_g and n_e are equivalent. Figs. 1 and 2 highlight that K_g/K_e decreases as K_e increases, and n_g/n_e decreases as n_e increases. The data points in Fig. 2 are more concentrated than the data points in Fig. 1, whereas n_g is more concentrated than K_g . The n_g values for the 33 types of rockfills are distributed over the range of 0.3–0.7. The results are slightly more comprehensive than the previous statistical results obtained by Professor Kong for 13 types of rockfills, which fall in the range of 0.4–0.6 [5]. The average value of n_g is 0.5, as indicated by the results of Professor Kong [5]. The n_e distribution falls in the range of 0.2–0.6, and higher n_e values typically correspond to higher n_g values. Thus, n_g/n_e values are distributed over the range of 1.0–2.2 and are concentrated in a smaller range with an increasing n_g . Conversely, the distribution of K_g/K_e values is slightly affected by the K_g values.

The equations for the best-fit curves of the date in Fig. 1 and Fig. 2 are:

$$\frac{K_g}{K_e} = 1 + \frac{a_1 - 1}{1 + (K_e/b_1)^{m_1}}, \quad \frac{n_g}{n_e} = 1 + \frac{B_1 - 1}{1 + (n_e/B_2)^{6.681}}, \quad (7)$$

where a_1 , b_1 , m_1 , B_1 , and B_2 are the fitting parameters. The best-fit curve and the best-fit curve \pm one and two standard deviations (SD) are also shown in Figs. 1 and 2. The fitting parameters are listed in Table 4.

Table 4. Fitting parameters of G_{max} statistic curves

Statistic curves	a_1	b_1	m_1	B_1	B_2
Best-fit	10.067	209	1.069	1.645	0.417
Best-fit + 1 SD	9.000	366	1.892	1.892	0.424
Best-fit - 1 SD	11.775	133	1.398	1.398	0.402
Best-fit + 2 SD	8.936	530	1.061	2.145	0.426
Best-fit - 2 SD	15.300	126	1.960	1.150	0.350

The scatter of the data is difficult to resolve by the existing analysis because particle material, particle gradation, density, and soil skeleton structure may influence K_g and K_e . The K_e and n_e of rockfill used in dams can be determined according to the triaxial tests or the back-analysis using the prototype monitoring. The K_g and n_g can be determined by Eq. (7) with the best-fit curve, and sensitivity analysis can be applied with the best-fit curve \pm one and two SD. Thus, G_{max} can be analogized according to the developed statistical relationship, which avoids the dynamic test. Furthermore, the analogized G_{max} would reflect the influence of the construction in situ, if the K_e and n_e are determined by the back-analysis using the prototype monitoring.

3. The analogy method of $G_{max} \sim \gamma$ and $\xi \sim \gamma$

In the past several decades, many researchers have explored $G/G_{max} \sim \gamma$ and $\xi \sim \gamma$ of soil and have developed the ranges of shear moduli and damping ratios for cohesive soil, sand, gravel, and rockfill [3–5]. The author gathered dynamic characteristics of numerous rockfills in earth-rockfill dams both in China and abroad, developed $G/G_{max} \sim \gamma$ and $\xi \sim \gamma$ statistic curves for rockfill, and applied them in the dynamic analysis of two small- to middle-scale CFRDs. The details are presented in the paper “Application of rockfill dynamical characteristic statistic curve in

mid-small scale concrete face dam dynamic analysis”, which was published in the 15WCEE. The statistic curves of and can be expressed as:

$$\frac{G}{G_{max}} = b + \frac{1-b}{1 + \left(\frac{\gamma}{x_0}\right)^m}, \quad \xi = A_2 + \frac{A_1 - A_2}{1 + a\gamma^n}, \quad (8)$$

where b is minimum G/G_{max} versus γ between 10^{-6} - 10^{-1} ; A_1 and A_2 are maximum ξ and minimum ξ , respectively, versus γ between 10^{-6} and 10^{-1} ; and x_0 , m , a , and n are fitting parameters. The parameters are presented in Table 5.

Table 5. Parameters for $G/G_{max} \sim \gamma$ and $\xi \sim \gamma$ statistic curves

Statistic curves	b	x_0	m	A_1	A_2	a	n
Best-fit	0.0912	0.0305	0.8522	0.0082	0.2612	2.9029	0.6417
Best-fit + 1 SD	0.0935	0.0581	0.8970	0.0121	0.2920	3.9535	0.6556
Best-fit - 1 SD	0.0842	0.0160	0.8421	0.0042	0.2180	1.9753	0.6186
Best-fit + 2 SD	0.1109	0.0967	1.0888	0.0153	0.3251	5.2038	0.6816
Best-fit - 2 SD	0.0796	0.0088	0.8388	0.0008	0.1847	1.3052	0.5871

Thus, the dynamic characteristics of the rockfill used in the dam can be determined; G_{max} can be analogized according to E_0 and G_{max} statistic curves; and $G/G_{max} \sim \gamma$ and $\xi \sim \gamma$ can be analogized by the statistic curves. To examine the effectiveness, this study applied the dynamic analysis of a middle-scale CFRD whose rockfill dynamic parameters were analogized according to the proposed method.

4. Application

The Malutang II CFRD is located along the Panlong River in the Yunnan province of China. Along the crest, the dam is 154 m high and 493.4 m long; the upstream dam slope is 1:1.4, and the downstream integrated dam slope is 1:1.3. The total reservoir capacity is $5.36 \times 10^8 \text{ m}^3$, and the install capacity is 300 MW. The design intensity of the Malutang II is 7.0 degree. So according to conditions of the specifications listed in Table 1, the Malutang II degsign intensity equal 7.0 degree, and the reservoir is less than 10^9 m^3 , and the install capacity is less than 1,200 MW, which don't need to take dynamical analysis with the FEM. However, according to the new order, the Malutang II reservoir is more than 10^8 m^3 , and the install capacity is larger than 300 MW, which should take dynamical analysis with the FEM. A typical section of the CFRD is provided in Fig. 3.

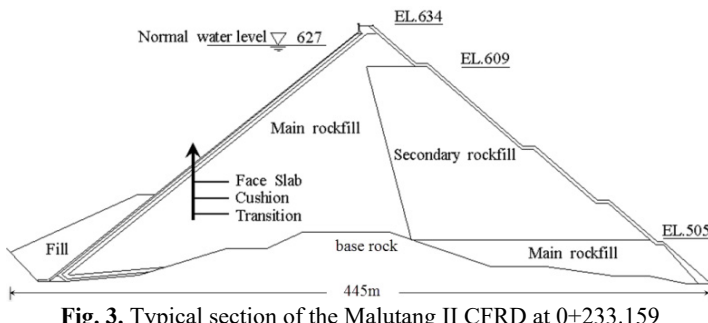


Fig. 3. Typical section of the Malutang II CFRD at 0+233.159

4.1. E_0 back analysis according to prototype monitoring

The three-dimensional FE mesh of Malutang II is shown in Fig. 4. The three-dimensional FE

mesh is composed of 8,284 elements. The rockfills, cushion, transition, and concrete face slabs were simulated by four-, six-, and eight-node isoparametric spatial elements. A detailed settlement monitoring system was established to monitor the deformation of the Malutang II CFRD [24]. Vertical displacements inside the dam body were measured by settlement gauges distributed throughout typical cross-sections at 0+233.159. Twenty-two hydraulic overflow settlement gauges along three monitoring lines were placed in the typical sections, of which 19 survived (at elevations of 522, 556, and 590 m). Two other monitoring gauges, for monitoring settlement and horizontal displacement, were distributed on the downstream slope of the typical section at elevations 565 and 595 m. The layout of displacement gauges in the typical section is presented in Fig. 5.

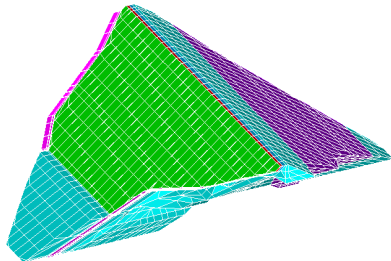


Fig. 4. Three-dimensional FE mesh

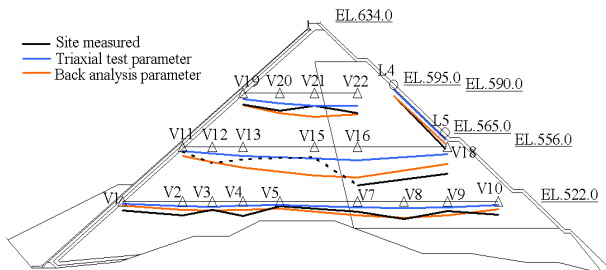


Fig. 5. Comparison of simulations and site measurements

The site-measured displacements and construction record indicated that rapid construction reduced the time of consolidation [24], modified the structure of the rockfill, and caused the rockfill density to be unevenly distributed. The uneven density of the rockfill affected the rockfill deformation modulus and the dam body displacement. According to the construction record, the main rockfill and the secondary rockfill were separated into three parts corresponding to the three construction rates. Thus, the main rockfill types I, II, and III represent the main rockfill types that are constructed in stages I, II, and III & IV, respectively. The same notation is applied for secondary rockfill. The fill zone material was simulated using secondary rockfill II in the back-analysis. Therefore, Duncan and Chang's *E-B* model parameters K_e , n_e , R_f , φ_0 , $\Delta\varphi$, K_b , and m of the main rockfill and the secondary rockfill in these construction periods were back-analyzed. The details of the *E-B* model parameters back-analysis are listed in the reference [24]. The results of the back-analysis are shown in Table 6. The FEM analysis was conducted using model parameters obtained from the back-analysis. The displacements calculated from the back-analysis parameters are also shown in Fig. 5. The settlements calculated using the back-analysis parameters are consistent in magnitude and distribution with the values measured in situ. Therefore, in general, the back-analysis results satisfactorily reflect the deformation properties of the dam.

Table 6. The back-analyzed *E-B* parameters of Malutang rockfill [24]

Methodology	Material	K_e	n_e	R_f	φ_0	$\Delta\varphi$	K_b	m
Triaxial test	Main rockfill	1,467	0.38	0.80	55.0	15.0	1,570	0.23
	Secondary rockfill	1,042	0.53	0.75	50.7	10.5	933	0.08
	Cushion	1,963	0.35	0.74	55.5	13.2	1,742	0.21
	Transition	1,583	0.35	0.74	57.6	16.5	1,590	0.16
	Fill	1,042	0.53	0.75	50.7	10.5	933	0.08
Back-analysis	Main rockfill I	1,011	0.33	0.90	55.0	16.0	1,112	0.22
	Main rockfill II	712	0.40	0.85			422	0.45
	Main rockfill III	1,545	0.18	0.60	50.0	5.0	1,663	0.47
	Secondary rockfill I	901	0.22	0.62			517	0.15
	Secondary rockfill II	311	0.20	0.90			207	0.05
	Secondary rockfill III	1,200	0.31	0.60			558	0.32

4.2. Analogy of the dynamic characteristics

In the dynamic analysis, an equivalent nonlinear viscoelastic model was employed. In this model, the dynamic shear modulus and damping ratio are calculated as:

$$\frac{G}{G_{max}} = \frac{1}{1 + k_1 \bar{\gamma}}, \quad \xi = \xi_{max} \frac{k_1 \bar{\gamma}}{1 + k_1 \bar{\gamma}}, \quad \bar{\gamma} = \frac{\gamma}{(\sigma'_0/P_a)^{1-n_g}}, \quad G_{max} = K_g P_a \left(\frac{\sigma'_0}{P_a} \right)^{n_g}, \quad (9)$$

where $\bar{\gamma}$ is the normalized shear strain and k_1 and ξ_{max} are the model parameters. The parameters K_g and n_g are determined by Eq. (7) according to the best-fit curve and the *E-B* model parameters determined by back analysis in Table 6. The analogized $G/G_{max} \sim \gamma$ and $\xi \sim \gamma$ curves of the rockfill are plotted in Figs. 6 and 7.

The normalized shear strain $\bar{\gamma}$ reflects the influence of the mean effective stress on the damping ratio. The $\xi \sim \gamma$ curves with mean effective stresses of 100 and 1,600 kPa are plotted in Fig. 7. The $G/G_{max} \sim \gamma$ and $\xi \sim \gamma$ curves of the soil reflect the energy transformation mechanism under dynamic loading. Higher soil skeletal stiffness can store more elastic energy and produce a smaller damping ratio, which is the ratio between the lost energy and stored energy. However, the rockfill structure is more complex, and many factors influence energy transformation. Friction among soil particles, pore-fluid flow, and particle breakage consume energy generated by dynamic loading. Denser rockfill produces a stronger soil skeleton and higher G .

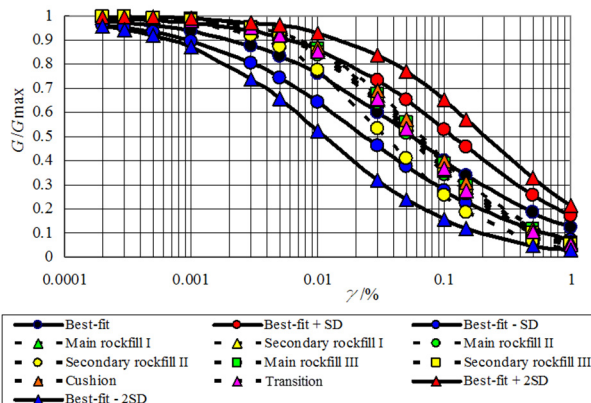


Fig. 6. Analogized $G/G_{max} \sim \gamma$ of the rockfill in the Malutang II CFRD

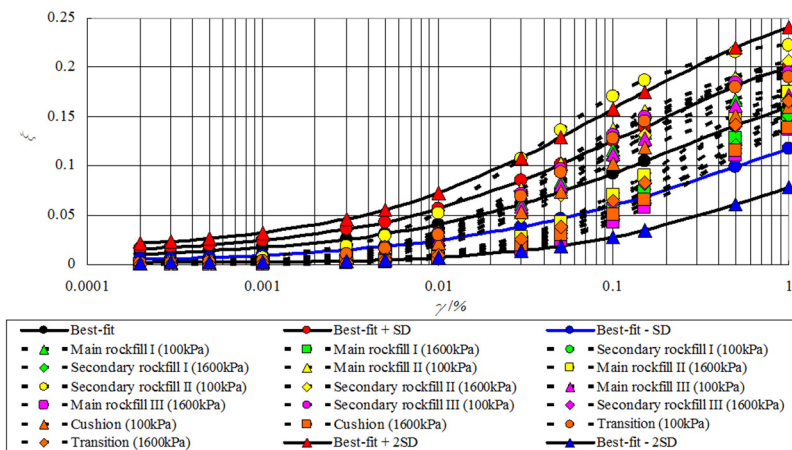


Fig. 7. Analogized $\xi \sim \gamma$ of the rockfill in the Malutang II CFRD

However, denser rockfill also generates additional particle contacts, greater dissipated energy, and a higher damping ratio [3]. The E - B model parameters for the rockfill determined by back analysis indicated that small K_e values generate high n_e values. A small K_e indicated that the soil exhibited a looser structure or contained softer particles. A large n_e indicated that the soil exhibited a flexible skeleton and sensitivity to stress [25]. The site monitoring and back analysis results indicated that different densities significantly influenced the deformation modulus of the rockfill. Denser rockfill produced higher G and ξ values [3]. The analogized G_{max} parameters K_g and n_g also conformed to the rules. Thus, the analogized curves with a mean effective stress of 100 kPa, as shown in Fig. 7, are all located above the best-fit curve even if the analogized K_g is higher than the average values of the compiled rockfill. The largest damping ratio of the secondary rockfill II is maintained under the best-fit curve + 2 SD because the analogized K_g is larger than the smallest value for the compiled rockfill. In this context, a higher G_{max} produces a lower $\xi \sim \gamma$ curve and a higher $G/G_{max} \sim \gamma$ curve, which conform to the general rules. The analogized dynamic parameters are listed in Table 7.

Table 7. The analogized dynamic parameters

Material	K_e	k_1	n_g	ξ_{max}
Main rockfill I	2,445	16.3	0.51	0.188
Main rockfill II	2,083	19.0	0.55	0.210
Main rockfill III	3,022	15.8	0.30	0.182
Secondary rockfill I	2,317	17.6	0.36	0.203
Secondary rockfill II	1,426	29.0	0.33	0.230
Secondary rockfill III	2,655	18.0	0.49	0.202
Cushion	3,053	15.0	0.54	0.171
Transition	2,371	17.4	0.53	0.201
Fill	2,280	18.0	0.49	0.205

4.3. Earthquake wave

According to the geological inspection, the intensity of the design earthquake for the Malutang II dam with a transcendental probability of 5 % for 50 years is 7.0 and the peak acceleration of ground motion is 0.05 g. The transcendental probability for the check earthquake for 100 years is 5 %, and the acceleration of the ground motion is 0.095 g. The earthquake waves, which were applied in an upstream-downstream direction, vertical direction, and dam axis direction, are displayed in Fig. 8.

4.4. Dynamic response of the dam

The earthquake time-step in the calculations was 0.02 s, and the acceleration in the vertical direction was reduced to two thirds. The acceleration responses of the Malutang II CFRD are presented in Fig. 9. The acceleration responses demonstrate that the maximum accelerations of the two earthquakes in every direction are located on the top of the dam. The maximum accelerations of the design earthquake in the upstream-downstream direction, vertical direction, and dam axis direction are 0.235, 0.137, and 0.173 g, respectively. The acceleration amplifications are 4.70, 4.11, and 3.46. The values of the check earthquake are 0.275, 0.187, and 0.189 g. The acceleration amplifications are 2.89, 2.96, and 1.99. The dynamic FEM results indicate that the maximum accelerations of the dam increase with the maximum accelerations of the earthquake and that the acceleration amplifications decrease with the maximum accelerations of the earthquake, which correspond to the earthquake response and the dynamic FEM analysis response of the same type of CFRD [17, 20-22, 28, 29].

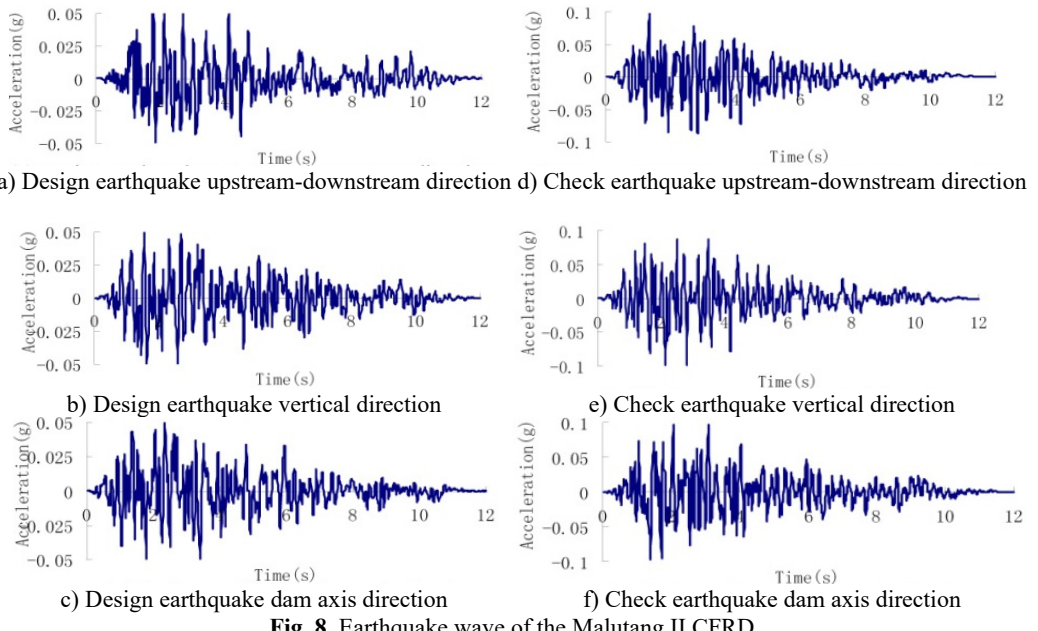


Fig. 8. Earthquake wave of the Malutang II CFRD

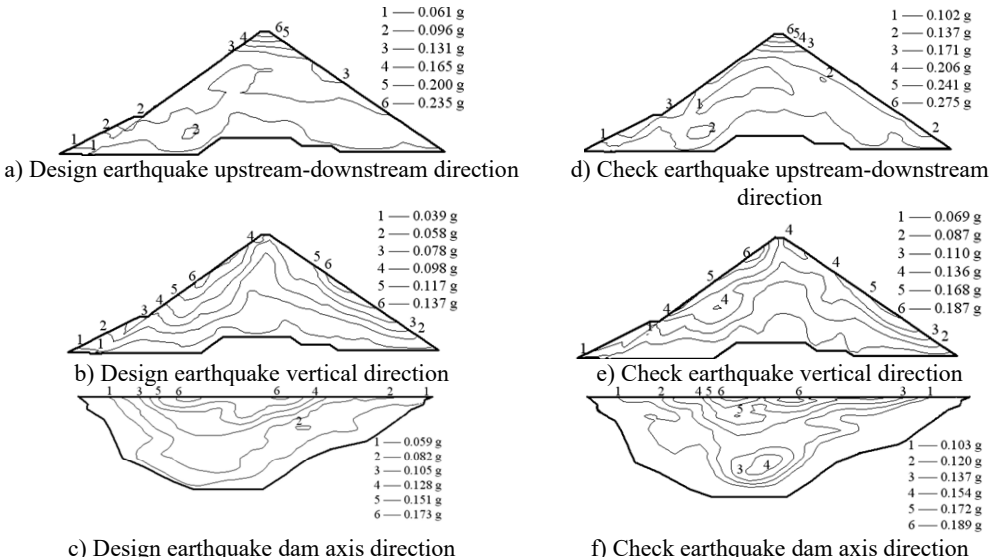


Fig. 9. Acceleration of the Malutang II CFRD

The dynamic stresses on the concrete face-slab of the design and check earthquakes are presented in Figs. 10 and 11, respectively. The maximum face-slab dynamic stresses of the design and check earthquakes are both located in the middle area. The maximum dynamic compression and tensile stresses along the dam slope for the design earthquake are 2.695 and 2.958 MPa (compression is positive). The stresses along the dam axis are 0.8 and 1.075 MPa. Check earthquake stresses along the dam slope are 4.369 and 3.353 MPa. The stresses along the dam axis are 1.558 and 1.644 MPa. The slab dynamic stresses increase with the maximum acceleration of the earthquake. The maximum compression stress and tensile stress are nearly equivalent; the stress along the dam slope is larger than the stress in the dam-axis direction, because the slit joints among face slabs release the part of the dynamic deformation in the face slab along the dam axis.

As indicated by the acceleration response and distribution of the maximum face-slab dynamic stresses, the results of the dynamic analysis for the Malutang II CFRD conformed to the general rules, which were shown in the earthquake response and the dynamic FEM analysis response of the same type of CFRD [17, 20, 21, 22, 29].

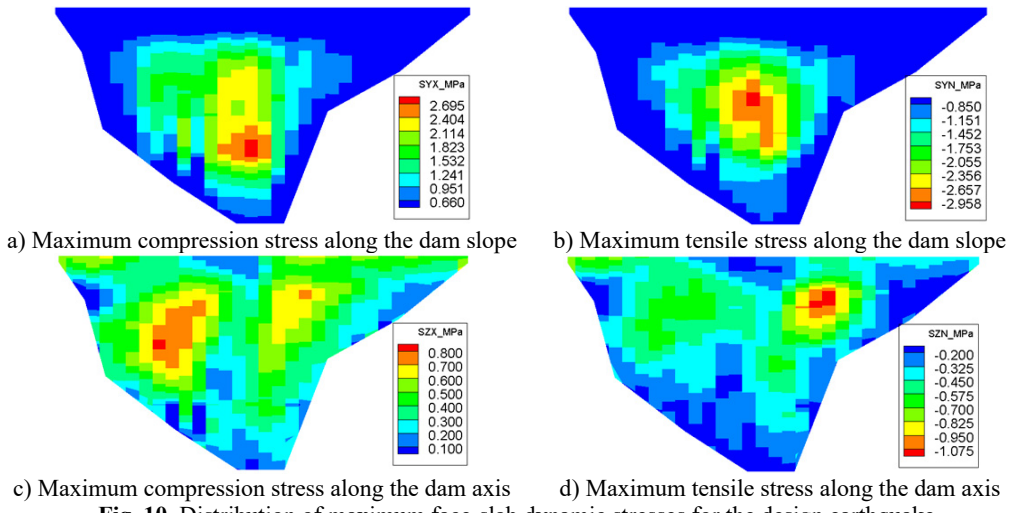


Fig. 10. Distribution of maximum face-slab dynamic stresses for the design earthquake

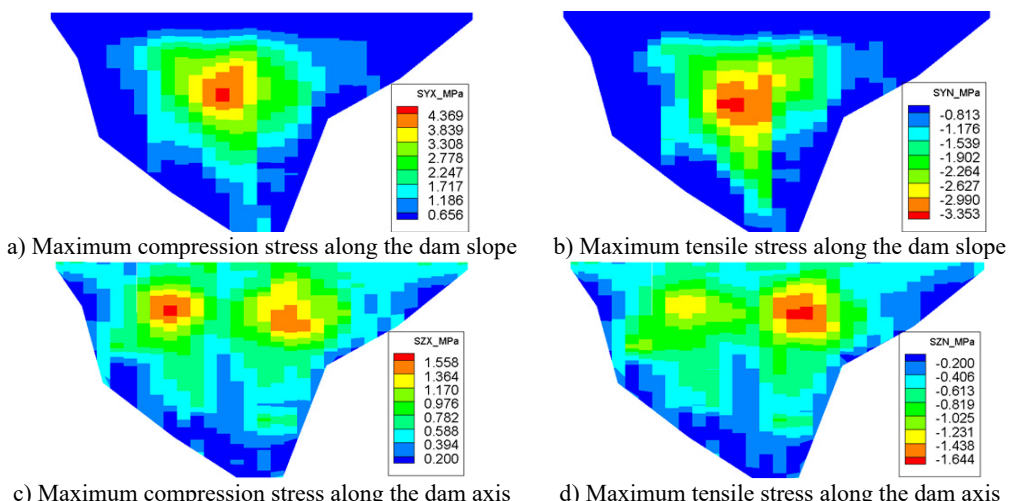


Fig. 11. Distribution of maximum face-slab dynamic stresses for the check earthquake

5. Conclusions

According to prototype monitoring of the earth-rockfill dam, E_0 of the rockfill were determined by back analysis, which reflected the influences of construction and particle size effect. The G_{max} of rockfill can be analogized according to the statistical relationship and E_0 . According to $G/G_{max} \sim \gamma$ and $\xi \sim \gamma$ statistic curves, E_0 , and the analogized G_{max} , the $G/G_{max} \sim \gamma$ and $\xi \sim \gamma$ curves of the rockfill were analogized.

The dynamic characteristics of the soil in the Malutang II CFRD were determined by the analogy method. Dynamic analyses by the FEM were performed for a design earthquake and check earthquake. The two earthquake waves exhibited different response spectrums and maximum accelerations. The dynamic responses of the dam conformed to general rules, which

were shown in the earthquake response and the dynamic FEM analysis response of the same type of CFRD. It indicates that the analogy method for dynamic characteristics is effective for rockfill and can be employed in a seismic safety check or reinforcement design of a small- to middle-scale earth-rockfill dam that cannot be analyzed by dynamic tests. The best-fit curves of the statistic relationships are the primary orientations for analogy. Furthermore, a sensitivity analysis of the dynamic parameters of rockfill can be determined according to the best-fit curve \pm one and two SD of the statistic relationships. The rockfill dynamic characteristics analogy method should be based on an analysis of the predominant influencing factors, such as dam prototype monitoring, construction records, and operation scenarios.

Acknowledgements

This research was supported by the National Natural Science Foundation of China (Nos. 51109027, 51179024, 51379029 and 51576029) and the Fundamental Research Funds for the Central Universities (No. DUT12LK11)

References

- [1] **Del Shannon A.** Dam Damage: Evaluating and learning from the Wenchuan earthquake's impact to China's dams. American Society of Civil Engineers, Oakland, CA, United States, 2009.
- [2] **Hardin B. O., Black W. L.** Vibration modulus of normally consolidated clay. Proceedings of ASCE, Vol. 94, Issue 2, 1968, p. 353-369.
- [3] **Seed H. Bolton, Wong Robert T., Idriss I. M., et al.** Moduli and damping factors for dynamic analyses of cohesionless soils. Journal of Geotechnical Engineering, Vol. 112, Issue 11, 1986, p. 1016-1032.
- [4] **Rollins K. M., Evans M. D., Diehl N. B., et al.** Shear modulus and damping relationships for gravels. Journal of Geotechnical and Geoenvironmental Engineering, Vol. 124, Issue 5, 1998, p. 396-405.
- [5] **Kong Xian-jing, Lou Shulian, Zou De-gao** The equivalent dynamic shear modulus and equivalent damping ratio of rockfill material for dam. Journal of Hydraulic Engineering, Vol. 8, 2001, p. 20-25.
- [6] **Hardin Bobby O., Kalinski Michael E.** Estimating the shear modulus of gravelly soils. Journal of Geotechnical and Geoenvironmental Engineering, Vol. 131, Issue 7, 2005, p. 867-875.
- [7] **Li Chong, He Chang-rong, Wang Chen, et al.** Study of scale effect of large-scale triaxial test of coarse-grained materials. Rock and Soil Mechanics. 2008, p. 563-566.
- [8] **Feng Zheng-yi, Tsai Pei-hsun, Li Jun-nan** Analyses of the dynamic responses of Li-yu-tan Earthdam subjected to Chi Chi earthquake. Journal of the Chinese of Soil and Water Conservation, Vol. 37, Issue 3, 1994, p. 271-289, (in Chinese).
- [9] **Duncan J. M., Byrne Peter, Wong Kai S., et al.** Strength, Stress-Strain and Bulk Modulus Parameters for Finite Element Analyses of Stresses and Movements in Soil Masses. University of California, Berkeley, Report No. UCB/GT/80-011980.
- [10] **Ju Lianyi** The Seismic Analysis and Seismic Design of Manla Rockfill Dam. Dalian University of Technology, Dalian, 2002, (in Chinese).
- [11] **Cheng Run-hu** Study on geological properties of rock-fill material in Zhangfeng reservoir. Journal of Water Resources and Architectural Engineering, 2010, p. 159-173., (in Chinese).
- [12] **Jia Gexu** Experimental Study on Enginerring Properties of Coarse-Grained Soils. Dalian University of Technology, Dalian, 2004, (in Chinese).
- [13] **Zhang Lin** Study on Influencing Factors of Embankment Dam Seismic Response. Hohai University, Nanjing, 2008, (in Chinese).
- [14] **Lu Tinghao, Shao Song Gui** 3-D Nonlinear FEM Analysis for TSQ-I Hydroelectric Project Concrete Face Rockfill Dam. Hongshui River, 1996, p. 20-23, (in Chinese).
- [15] **Ling Hua, Fu Hua, Han Hua-qiang, et al.** Experimental study on effects of particle breakage on static and dynamic characteristics of rock-fill materials. Journal of Water Resources and Architectural Engineering, 2010, p. 44-47, (in Chinese).
- [16] Institute of Earthquake Engineering Dalian University, Technology of Static and Dynamic Analysis of Core Rock-fill Dam of Shuangjiangkou Hydropower Station. Dalian University of Technology, Dalian, 2008, (in Chinese).

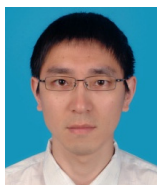
- [17] **Shen Zhenzhong, Xu Liqun, Wang Wei** Earthquake response of Xieka concrete face rockfill dam by FEM. American Society of Civil Engineers, Honolulu, HI, United States, 2010.
- [18] **Han Guo-cheng, Luan Mao-tian, Liu Wen-ting, et al.** Three-dimensional nonlinear analysis of seismic response of Pubugou cored rockfill dam. Journal of Dalian University of Technology, 2000, p. 218-233, (in Chinese).
- [19] Institute of Earthquake Engineering Dalian University, Technology of Static and Dynamic Analysis of Core Rock-fill Dam of Changheba Hydropower Station. Dalian University of Technology, Dalian, 2008, (in Chinese).
- [20] **Ren Jinke** Finite Element Analysis of Xi Liu Shui Face Rockfill Dam. Xi'an University of Technology, Xi'an, 2006, (in Chinese).
- [21] **Kong Xianjing, Zhou Yang, Zou Degao, et al.** Numerical analysis of dislocations of the face slabs of the Zipingpu concrete faced rockfill dam during the Wenchuan earthquake. Earthquake Engineering and Engineering Vibration, 2011, p. 581-589.
- [22] **Zhao Yixin** The Finite Element Analysis for Dynamic Stress and Deformation Characteristics of High Concrete-Face Rockfill Dam Built in Deep Alluvial Deposit. Xi'an University of Technology, Xi'an, 2009, (in Chinese).
- [23] **Chi ShiChun, Kong XianJing, Li JunJie** Research on Computation Theory of Core Rockfill Seismic Response Analysis and Aseismatic Measures. Report 4 of Science and Technology Project of State Grid Corporation of China. Dalian University of Technology, 2006, (in Chinese).
- [24] **Jia Yufeng, Chi Shichun** Back-analysis of soil parameters of the Malutang II concrete face rockfill dam using parallel mutation particle swarm optimization. Computers and Geotechnics, Vol. 65, 2015, p. 87-96.
- [25] **Wang Y. H., Siu W. K.** Structure characteristics and mechanical properties of kaolinite soils. II. Effects of structure on mechanical properties. Canadian Geotechnical Journal, Vol. 43, Issue 6, 2006, p. 601-617.
- [26] **Gu Ganchen, Shen Changsong, Cen Weijun** Earthquake Engineering for Earthrock Dams. China Water Power Press, Beijing, 2009, (in Chinese).
- [27] **Zhou G., Liu X., Zhao J., Liu Q., Yang Y., Yang Z.** The shaking table model test study on acceleration seismic response of Zipingpu CFRD. China Civil Engineering Journal, Vol. 45, 2014, p. 20-24, (in Chinese).
- [28] **Zou D., Xu B., Kong X., Liu H., Zhou Y.** Numerical simulation of the seismic response of the Zipingpu concrete face rockfill dam during the Wenchuan earthquake based on a generalized plasticity model. Computers and Geotechnics, Vol. 49, 2013, p. 111-122.



Yufeng Jia received Ph.D. degree in Structural Engineering from Dalian University of Technology, Dalian, China, in 2009. He is currently a Lecturer with the Institute of Earthquake Engineering, Dalian University of Technology. His current research interests include particle breakage of the coarse granular soil, soil constitutive model, and soil parameters back-analysis.



Shichun Chi received Ph.D. degree in Hydro-Structure from Hohai University, Nanjing, China, in 1995. From 1996 to 1998, he was a post-doctoral fellow in the Institute of Earthquake Engineering in Dalian University of Technology. From 1998, he was the Professor with the Institute of Earthquake Engineering, the second Director of the State Key Laboratory of Coastal and Offshore Engineering in Dalian University of Technology, China. His research interests include soil constitutive mode, seismic resistance of nuclear power plants, numerical analysis of earth rockfill dam.



Biao Xiang received Ph.D. degree in Hydro-Structure from Dalian University of Technology, Dalian, China, in 2009. He is currently a senior engineer, the second Director of the Hydro-structure Design Institute in POWERCHINA Kunming Engineering Corporation, Kunming, China.